Journal of Materials Chemistry A

COMMUNICATION

View Article Online
View Journal | View Issue

Cite this: J. Mater. Chem. A, 2015, 3, 19277

Received 27th July 2015
Accepted 25th August 2015

DOI: 10.1039/c5ta05793k

www.rsc.org/MaterialsA

Physical vapor deposition of amorphous MoS_2 nanosheet arrays on carbon cloth for highly reproducible large-area electrocatalysts for the hydrogen evolution reaction†

Xing Zhang, Yun Zhang, Bin-Bin Yu, Xing-Liang Yin, Wen-Jie Jiang, Yan Jiang, Jin-Song Hu* and Li-Jun Wan*

Molybdenum sulfide materials have been shown to be promising non-precious metal catalysts for the hydrogen evolution reaction (HER). This work reports a facile and scalable preparation method for amorphous MoS_2 nanosheet arrays directly deposited on carbon cloth (a-MoS_2 NA/CC) using a highly reproducible physical vapor deposition (PVD) approach. As a result of the three-dimensional nanostructure of the catalyst, the amorphous nature and the abundant exposed edge sites of MoS_2, the a-MoS_2 NA/CC composite exhibited superior catalytic activity and stability for the HER in acidic solutions.

Hydrogen as a clean, efficient energy carrier has been extensively pursued and considered as a promising alternative to traditional fossil fuels for the future by virtue of its high energy density and the zero environmental impact of the combustion product.[1,2] Electrocatalytic systems are one of the most important ways for H_2 generation, where platinum and its alloys are the most effective catalysts with a significant rate at a very low overpotential.[3,4] However, the high material costs and limited resource of these catalysts hinder the practical applications of electrochemical H_2 generation. Consequently, the ongoing search for efficient alternatives composed of low-cost materials is crucial for a sustainable 'hydrogen economy'.

Plenty of non-noble metal materials have been exploited for catalyzing the hydrogen evolution reaction (HER), including transition metal sulfides,[5–8] selenides,[9,10] carbides,[11,12] phosphides,[13–15] and nitrides,[16,17] as well as some combinations.[18–20] Among all these materials, molybdenum disulfide (MoS_2), two-dimensional sheets of vertically stacked S–Mo–S interlayers, has been drawing broad attention due to its high activity and low-cost, earth-abundant composition since Norskov and coworkers reported the catalytic activity of MoS_2 nanoparticles for the HER.[21] Tremendous effort has been devoted to developing multifarious MoS_2-based HER electrocatalysts in the form of crystalline[10,22,23] or amorphous states,[24–27] and even molecular mimics[28] during the past few years. It was reported that amorphous MoS_2 exhibited a better electrocatalytic performance than the crystalline version due to more defects and catalytically active sites. However, MoS_2 exhibits a poor intrinsic conductivity, which severely suppresses charge transport and thus the electrocatalysis efficiency.[29] The practical applications of these catalysts demand that the catalysts are grafted onto conductive substrates using polymer binders as film-forming agents, which will block some of the active sites and deteriorate the mass diffusion,[30] thus causing degradation of the catalytic activity. Therefore, developing nanostructured MoS_2 that is directly self-supported on a highly conductive substrate with a large surface area is desirable to improve its electrocatalytic activity in practical applications.[31,32] It was recently reported that depositing MoS_2 nanoparticles on graphene was effective to enhance their electrocatalytic performance for the HER.[33,34] Carbon cloth (CC) possesses a high electrical conductivity, a large surface-area, excellent chemical stability, maneuverability and flexibility, making it an ideal support to construct functional nanostructures for applications in electrochemical energy conversion and storage.

Herein, a reproducible physical vapor deposition approach was developed to prepare large-area amorphous MoS_2 nanostructures supported on carbon cloth. The morphology of the MoS_2 nanostructures could be easily tuned by the deposition power of the PVD. As a result of the three-dimensional nanostructure of the catalyst, the amorphous nature and the abundant exposed edge sites of MoS_2, the MoS_2 nanosheet arrays on CC demonstrated an excellent catalytic performance and long-term stability for the HER in acidic solutions. The reported approach provides a facile way to explore new nanostructured electrocatalysts for applications involving water splitting and energy conversion.

Beijing National Laboratory for Molecular Sciences, Key Laboratory of Molecular Nanostructure and Nanotechnology, Institute of Chemistry, Chinese Academy of Sciences (CAS), 2 North 1st Street, Zhongguancun, Beijing 100190, P. R. China. E-mail: hujs@iccas.ac.cn; wanlijun@iccas.ac.cn; Fax: +86 10 82613929

† Electronic supplementary information (ESI) available: Descriptions of experimental methods, elemental analysis, TEM images, XPS spectra, and XRD patterns. See DOI: 10.1039/c5ta05793k

MoS_2 nanostructures with different morphologies were prepared by the physical vapor deposition of MoS_2 directly on carbon cloth *via* a magnetron sputtering system. It was found that well-defined nanosheet arrays could be obtained when using a sputtering power of 100 W at a gas pressure of 3 mtorr. Fig. 1a is a typical optical image of the obtained product. The uniform colour indicates that molybdenum sulfide is distributed evenly on the surface of the carbon cloth. The size of the product is dependent on the substrate size of the magnetron sputtering system. The composition and crystal structure of the product were first investigated by the X-ray diffraction (XRD) technique. Fig. 1b presents typical XRD patterns of the product and the bare CC. By comparing the two patterns, it can be seen that all of the recorded diffraction peaks in the XRD pattern of the synthesized product can be indexed to the diffraction peaks from the CC. The only difference is the decreased intensities of the peaks, implying the formation of a MoS_2 layer on the CC and the amorphous nature of MoS_2 in the product. The EDS spectrum (Fig. S1†) shows that the product is composed of C, Mo and S elements, and the atomic ratio of Mo : S is 1 : 2, corroborating that the product contains MoS_2. Fig. S2† shows the transmission electron microscopy (TEM) images of the MoS_2 nanosheets coated on the surface of the CC. A typical lamellar structure of MoS_2 with a lattice spacing of 0.62 nm was observed from the TEM image, which is consistent with the interlayer spacing of MoS_2. Meanwhile, no obvious lattice fringes were found during the TEM observations, corroborating that these MoS_2 nanosheets were not well-crystallized. This result is consistent with the XRD measurements. It has been demonstrated that amorphous MoS_2 usually exhibits a higher HER activity than the crystalline version due to the larger number of exposed edges in the amorphous structure.[25,35,36] Therefore, it is expected that the nanometer sized, amorphous MoS_2 nanosheets supported on the CC here could provide more abundant edges and catalytically active sites. In order to further investigate the chemical nature and bonding state of MoS_2 on the CC surface, the X-ray photoelectron spectroscopy (XPS) spectrum was recorded. Fig. 1c depicts the high-resolution XPS signals of Mo 3d with two characteristic peaks at 229.3 and 232.4 eV, which arise from Mo^{4+} $3d_{5/2}$ and $3d_{3/2}$ orbitals, respectively. This result suggests that Mo^{4+} dominates in the product. The S 2p spectrum (Fig. 1d) shows a single doublet with a binding energy of 162.2 and 163.2 eV, which is attributed to the sulfide (S^{2-}) ligand in MoS_2.[22] These results confirmed the existence of MoS_2 in the product.

The scanning electron microscopy (SEM) image (Fig. 2a) clearly shows that sheet-like structures ~60 nm wide and ~2 nm thick were vertically grown on the fiber of the carbon cloth and cross-linked together. The corresponding energy dispersive X-ray (EDS) elemental mapping images of elemental Mo, S and C shown in Fig. 2d clearly show that both Mo and S elements are uniformly distributed throughout the whole nanosheet array. Therefore, all the above evidence indicates that the whole area of the CC is covered with densely packed amorphous MoS_2 nanosheet arrays (a-MoS_2 NA/CC).

It is well known that the morphology and size of nanostructures significantly influence the performance of

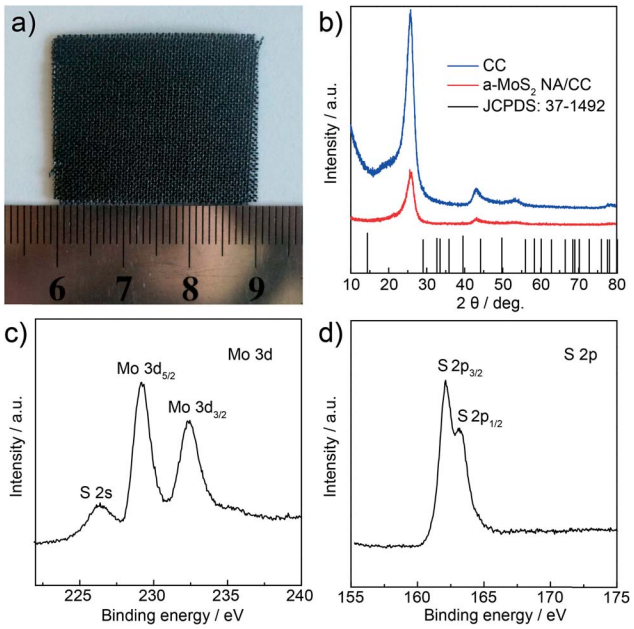

Fig. 1 (a) Optical image of the synthesized a-MoS_2/CC; (b) XRD patterns of a-MoS_2/CC and bare carbon cloth with a standard pattern of hexagonal MoS_2 crystals (JCPDS 37-1492) as a reference; (c) and (d) high resolution XPS signals of Mo 3d and S 2p, respectively.

nanomaterials, especially for electrocatalysis, since the electrocatalytic activity of a catalyst is closely related to the amount of catalytically active sites on its surface. In order to investigate the capability of tuning the morphology of a-MoS_2 NA/CC *via* the simple PVD method reported here, and thus optimize its electrocatalytic performance for the HER, a series of experiments were carried out by changing the deposition conditions, such as the sputtering power. It was interestingly found that the morphologies of the MoS_2 nanostructures were closely correlated to the sputtering power. The typical SEM images of two samples prepared under the same conditions except for using 70 W and 150 W sputtering powers are shown in Fig. 2b and c. Although the XRD results show that both products are composed of amorphous MoS_2 (Fig. S3†), the products display different morphologies compared to that of the sample prepared at 100 W. Unlike the densely compacted nanosheet arrays prepared at 100 W (Fig. 2a), sparse short nanostructures were obtained at 70 W (Fig. 2b) and a film-like structure with smooth surface but no protruding sheet-like nanostructures was achieved when the sputtering power was increased to 150 W (Fig. 2c). These results indicate that the sputtering power significantly influences the morphology of the MoS_2 nanostructures.

Encouraged by the nanosheet morphology and amorphous structure of MoS_2, the synthesized a-MoS_2 NA/CC was directly used as a working electrode to explore its potential in HER applications. The catalytic activity of the a-MoS_2 NA/CC composite for the HER was evaluated in N_2 saturated 0.5 M H_2SO_4 solution and compared with the catalytic activity of bare CC, a-MoS_2/CC obtained at different sputtering powers, and the commercial Pt/C catalyst (20 wt% Pt, Johnson Matthey). The

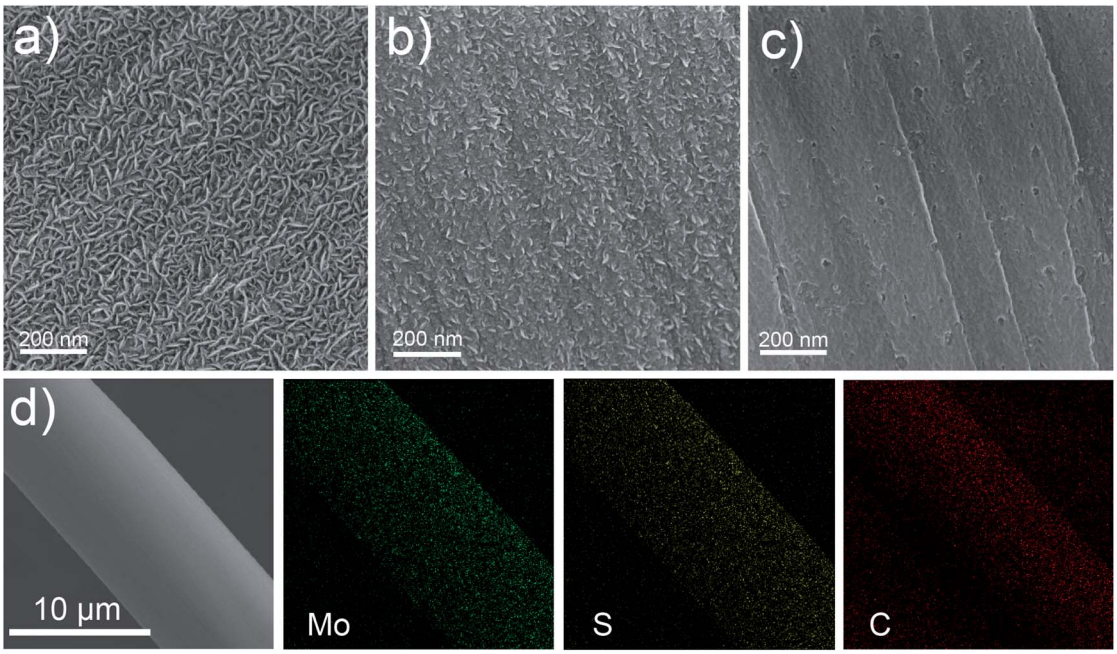

Fig. 2 SEM images of MoS_2 nanostructured films obtained at different sputtering powers: (a) 100 W; (b) 70 W; (c) 150 W; (d) SEM image and the corresponding EDS elemental mapping images of Mo, S and C for a-MoS_2 NA/CC at 100 W.

loading of MoS_2 was kept at 0.41 mg cm^{-2} for all three a-MoS_2/CC samples. Electrochemical measurements were carried out using the standard three-electrode setup with a saturated calomel electrode (SCE) as the reference electrode and a graphite rod as the counter electrode (see experimental section for details†). Fig. 3a shows the polarization curves of all the catalysts. Pt/C exhibits the expected HER activity with a near zero overpotential, while bare CC shows a very poor HER activity. The amorphous MoS_2 with a smooth, flat surface prepared at 150 W reveals a poor catalytic activity for the HER with an onset overpotential of 180 mV and an output current density of 10 mA cm^{-1} at an overpotential of 242 mV. All potentials are *versus* RHE. When the surface of the amorphous MoS_2 becomes rougher, *i.e.* the product obtained at a sputtering power of 70 W, an improved activity for the HER with a lower onset overpotential of 177 mV is observed. The best performance was achieved with a-MoS_2 NA/CC, which exhibits the smallest overpotential of 224 mV at a current density of 10 mA cm^{-2} and the largest cathodic current density at the same potential among the three a-MoS_2/CC catalysts. This catalytic activity is comparable to some of the best MoS_2 based HER catalysts that have been developed by other groups.[5,6] The enhancement of the electrocatalytic activity of a-MoS_2 NA/CC can be ascribed to the increase in the number of exposed edges of MoS_2 as catalytically active sites due to the structure of the nanosheet arrays vertically grown on the CC. It should be noted that magnetron sputtering deposition is a highly reproducible method. During the experiments, it was found that almost exactly the same results can be achieved when keeping the deposition conditions and catalyst loading exactly the same.

In order to understand the kinetics process of hydrogen evolution, the Tafel plots were calculated for all the catalysts by plotting the overpotential *versus* the current density in logarithmic scale (η *vs.* $\log j$), as shown in Fig. 3b.[37] The linear portions of the Tafel plots were fitted to the Tafel equation ($\eta = b \log j + a$, where j is the current density and b is the Tafel slope). The values of the Tafel slopes were estimated from Fig. 3b to be ~36 and ~58 mV per decade for Pt/C and a-MoS_2 NA/CC, respectively. It should be noted that the HER is a multi-step electrochemical process taking place on the surface of an electrode. There are three principle steps for converting H^+ to H_2 in the generally accepted reaction mechanism in acid solutions:[38,39]

$$H^+ + M + e \leftrightarrow H^*\text{–}M \text{ (Volmer reaction)} \quad (1)$$

$$H^*\text{–}M + H^+ + e \leftrightarrow H_2 + M \text{ (Heyrovsky reaction)} \quad (2)$$

$$2M\text{–}H^* \leftrightarrow H_2 + 2M \text{ (Tafel reaction)} \quad (3)$$

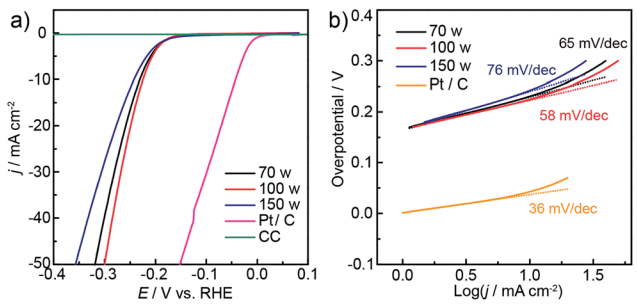

Fig. 3 Electrochemical measurements for the a-MoS_2 nanostructured film/CC composite catalysts in H_2SO_4 (0.5 M). (a) Polarization curves for bare CC, Pt/C, and a-MoS_2 nanostructured film/CC deposited with different sputtering powers at a scan rate of 2 mV s^{-1}. (b) Tafel plots for the a-MoS_2 nanostructured film/CC and Pt/C.

where H* represents a hydrogen atom chemically adsorbed on an active site of the electrode surface (M). The theoretical Tafel slopes for the typical Volmer, Heyrovsky, and Tafel reactions are 120 mV per decade, 40 mV per decade and 30 mV per decade, respectively.[10,40] In view of the Tafel slope of 58 mV per decade for a-MoS_2 NA/CC, a combination of the Volmer reaction, involving an electrochemical desorption step that converts protons into absorbed hydrogen atoms on the catalyst surface, and the Heyrovsky reaction, involving the formation of surface-bound hydrogen molecules, should dominate the HER on the surface of the a-MoS_2 NA/CC electrode.[41]

Moreover, the durability of the a-MoS_2 NA/CC composite was probed by continuous cyclic voltammetry (CV) sweeps for 1000 cycles between +280 and −319 mV *vs.* RHE at a scan rate of 100 mV s^{-1} in 0.5 M H_2SO_4 solution. At the end of the cycling, the catalyst was measured using the same applied potential range as the initial test. As shown in Fig. 4a, the current density of the a-MoS_2 NA/CC composite catalyst remained almost unchanged even after the continuous 1000 cycling (226 mV at 10 mA cm^{-2}), indicating the remarkable long-term stability of electrocatalytic activity. In addition, SEM analysis of a-MoS_2 NA/CC after the stability testing shows that the original morphology of the nanosheet arrays was well-maintained (Fig. 4b). XRD (Fig. S4†) and XPS (Fig. S5†) analyses also indicate no obvious changes in the crystalline structure before and after the durability test. These results validate the superior durability of a-MoS_2 NA/CC, which could be attributed to the direct integration of MoS_2 nanosheet arrays on the CC without any need for a polymer binder and strong interactions between the MoS_2 nanosheets and the CC in the one-step PVD procedure.[42] The carbon cloth not only facilitated fast electron transfer and collection, but also provided a monolithic self-supporting substrate, which enables the direct assembly of electrode for the HER. These results suggest the potentials of a-MoS_2 NA/CC as a low-cost and efficient hydrogen evolution cathode.

In summary, amorphous MoS_2 nanosheet arrays have been directly constructed on a conductive carbon cloth substrate *via* a facile and reproducible PVD approach. Benefiting from the amorphous nature of MoS_2 and the abundant exposed edge sites in the structure of the nanosheet arrays as well as the three-dimensional conductive structure of the catalyst, the synthesized a-MoS_2 NA/CC composite exhibited superior catalytic activity and durability for the HER in acidic solutions. These results suggest that this facile and easy scale-up process could be useful to explore monolithic MoS_2-based electrocatalysts or other low-cost, earth-abundant, and environmentally friendly materials for their potential application in the HER.

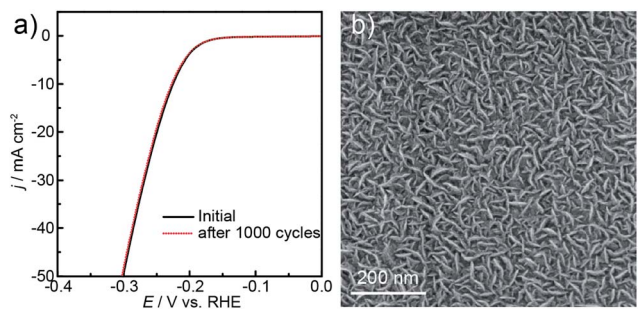

Fig. 4 (a) Polarization curves of a-MoS_2 NA/CC before and after 1000 cycles of CV scanning between +280 and −319 mV (*vs.* RHE); (b) SEM image of a-MoS_2 NA/CC after 1000 CV scans.

Acknowledgements

We gratefully acknowledge the support from the National Key Project on Basic Research (2015CB932302), the National Natural Science Foundation of China (91127044 and 21173237), and the Strategic Priority Research Program of the Chinese Academy of Sciences (Grant No. XDB12020100).

Notes and references

1 J. A. Turner, *Science*, 2004, **305**, 972–974.
2 M. S. Dresselhaus and I. L. Thomas, *Nature*, 2001, **414**, 332–337.
3 A. le Goff, V. Artero, B. Jousselme, P. D. Tran, N. Guillet, R. Métayé, A. Fihri, S. Palacin and M. Fontecave, *Science*, 2009, **326**, 1384–1387.
4 J. Greeley, T. F. Jaramillo, J. Bonde, I. Chorkendorff and J. K. Norskov, *Nat. Mater.*, 2006, **5**, 909–913.
5 J. Xie, J. Zhang, S. Li, F. Grote, X. Zhang, H. Zhang, R. Wang, Y. Lei, B. Pan and Y. Xie, *J. Am. Chem. Soc.*, 2013, **135**, 17881–17888.
6 J. Xie, H. Zhang, S. Li, R. Wang, X. Sun, M. Zhou, J. Zhou, X. W. Lou and Y. Xie, *Adv. Mater.*, 2013, **25**, 5807–5813.
7 Y. Sun, C. Liu, D. C. Grauer, J. Yano, J. R. Long, P. Yang and C. J. Chang, *J. Am. Chem. Soc.*, 2013, **135**, 17699–17702.
8 Y. D. Li, X. L. Li, R. R. He, J. Zhu and Z. X. Deng, *J. Am. Chem. Soc.*, 2002, **124**, 1411–1416.
9 D. S. Kong, H. T. Wang, Z. Y. Lu and Y. Cui, *J. Am. Chem. Soc.*, 2014, **136**, 4897–4900.
10 D. Kong, H. Wang, J. J. Cha, M. Pasta, K. J. Koski, J. Yao and Y. Cui, *Nano Lett.*, 2013, **13**, 1341–1347.
11 C. Wan, Y. N. Regmi and B. M. Leonard, *Angew. Chem., Int. Ed.*, 2014, **53**, 6407–6410.
12 L. Liao, S. N. Wang, J. J. Xiao, X. J. Bian, Y. H. Zhang, M. D. Scanlon, X. L. Hu, Y. Tang, B. H. Liu and H. H. Girault, *Energy Environ. Sci.*, 2014, **7**, 387–392.
13 J. Tian, Q. Liu, Y. Liang, Z. Xing, A. M. Asiri and X. Sun, *ACS Appl. Mater. Interfaces*, 2014, **6**, 20579–20584.
14 Z. Pu, Q. Liu, P. Jiang, A. M. Asiri, A. Y. Obaid and X. Sun, *Chem. Mater.*, 2014, **26**, 4326–4329.
15 J. Kibsgaard and T. F. Jaramillo, *Angew. Chem., Int. Ed.*, 2014, **53**, 14433–14437.
16 A. morozan, V. Goellner, A. Zitolo, E. Fonda, B. Donnadieu, D. Jones and F. Jaouen, *Phys. Chem. Chem. Phys.*, 2015, **17**, 4047–4053.
17 W.-F. Chen, K. Sasaki, C. Ma, A. I. Frenkel, N. Marinkovic, J. T. Muckerman, Y. Zhu and R. R. Adzic, *Angew. Chem., Int. Ed.*, 2012, **51**, 6131–6135.
18 K. Xu, F. Wang, Z. Wang, X. Zhan, Q. Wang, Z. Cheng, M. Safdar and J. He, *ACS Nano*, 2014, **8**, 8468–8476.

19 D. Merki, H. Vrubel, L. Rovelli, S. Fierro and X. Hu, *Chem. Sci.*, 2012, **3**, 2515–2525.
20 P. D. Tran, M. Nguyen, S. S. Pramana, A. Bhattacharjee, S. Y. Chiam, J. Fize, M. J. Field, V. Artero, L. H. Wong, J. Loo and J. Barber, *Energy Environ. Sci.*, 2012, **5**, 8912–8916.
21 B. Hinnemann, P. G. Moses, J. Bonde, K. P. Jorgensen, J. H. Nielsen, S. Horch, I. Chorkendorff and J. K. Norskov, *J. Am. Chem. Soc.*, 2005, **127**, 5308–5309.
22 J. Kibsgaard, Z. B. Chen, B. N. Reinecke and T. F. Jaramillo, *Nat. Mater.*, 2012, **11**, 963–969.
23 Z. B. Chen, D. Cummins, B. N. Reinecke, E. Clark, M. K. Sunkara and T. F. Jaramillo, *Nano Lett.*, 2011, **11**, 4168–4175.
24 C. G. Morales-Guio, S. D. Tilley, H. Vrubel, M. Gratzel and X. Hu, *Nat. Commun.*, 2014, 5.
25 J. D. Benck, Z. Chen, L. Y. Kuritzky, A. J. Forman and T. F. Jaramillo, *ACS Catal.*, 2012, **2**, 1916–1923.
26 D. Merki, S. Fierro, H. Vrubel and X. L. Hu, *Chem. Sci.*, 2011, **2**, 1262–1267.
27 C. G. Morales-Guio and X. Hu, *Acc. Chem. Res.*, 2014, **47**, 2671–2681.
28 H. I. Karunadasa, E. Montalvo, Y. J. Sun, M. Majda, J. R. Long and C. J. Chang, *Science*, 2012, **335**, 698–702.
29 Y.-H. Lee, X.-Q. Zhang, W. Zhang, M.-T. Chang, C.-T. Lin, K.-D. Chang, Y.-C. Yu, J. T.-W. Wang, C.-S. Chang, L.-J. Li and T.-W. Lin, *Adv. Mater.*, 2012, **24**, 2320–2325.
30 J. D. Roy-Mayhew, G. Boschloo, A. Hagfeldt and I. A. Aksay, *ACS Appl. Mater. Interfaces*, 2012, **4**, 2794–2800.
31 B. Hinnemann, P. G. Moses, J. Bonde, K. P. Jørgensen, J. H. Nielsen, S. Horch, I. Chorkendorff and J. K. Nørskov, *J. Am. Chem. Soc.*, 2005, **127**, 5308–5309.
32 J. Q. Tian, Q. Liu, A. M. Asiri and X. P. Sun, *J. Am. Chem. Soc.*, 2014, **136**, 7587–7590.
33 Y. G. Li, H. L. Wang, L. M. Xie, Y. Y. Liang, G. S. Hong and H. J. Dai, *J. Am. Chem. Soc.*, 2011, **133**, 7296–7299.
34 C. Lee, H. Yan, L. E. Brus, T. F. Heinz, J. Hone and S. Ryu, *ACS Nano*, 2010, **4**, 2695–2700.
35 D. Merki and X. L. Hu, *Energy Environ. Sci.*, 2011, **4**, 3878–3888.
36 T.-W. Lin, C.-J. Liu and J.-Y. Lin, *Appl. Catal., B*, 2013, **134–135**, 75–82.
37 T. F. Jaramillo, K. P. Jorgensen, J. Bonde, J. H. Nielsen, S. Horch and I. Chorkendorff, *Science*, 2007, **317**, 100–102.
38 Y. Zheng, Y. Jiao, M. Jaroniec and S. Z. Qiao, *Angew. Chem., Int. Ed.*, 2015, **54**, 52–65.
39 C. G. Morales-Guio, L. A. Stern and X. L. Hu, *Chem. Soc. Rev.*, 2014, **43**, 6555–6569.
40 Y.-H. Chang, C.-T. Lin, T.-Y. Chen, C.-L. Hsu, Y.-H. Lee, W. Zhang, K.-H. Wei and L.-J. Li, *Adv. Mater.*, 2013, **25**, 756–760.
41 W. Zhou, K. Zhou, D. Hou, X. Liu, G. Li, Y. Sang, H. Liu, L. Li and S. Chen, *ACS Appl. Mater. Interfaces*, 2014, **6**, 21534–21540.
42 C. Tang, Z. Pu, Q. Liu, A. M. Asiri and X. Sun, *Electrochim. Acta*, 2015, **153**, 508–514.